Magnetic and electronic properties of *B*-site-ordered double-perovskite oxide La_2CrMnO_6 thin films

K. Yoshimatsu,[1,*] J. Ishimaru,[1] K. Watarai,[1] K. Yamamoto,[2,†] Y. Hirata,[2] H. Wadati,[2,‡] Y. Takeda,[3] K. Horiba,[4,5]
H. Kumigashira,[4,5,6] O. Sakata,[5,7] and A. Ohtomo[1,5]
[1]*Department of Chemical Science and Engineering, Tokyo Institute of Technology, 2-12-1 Ookayama, Meguro-ku, Tokyo 152-8552, Japan*
[2]*Institute of Solid State Physics, University of Tokyo, Kashiwa, Chiba 277-8581, Japan*
[3]*Materials Sciences Research Center, Japan Atomic Energy Agency, 1-1-1 Kouto, Sayo-cho, Sayo-gun, Hyogo 679-5148, Japan*
[4]*Photon Factory, Institute of Materials Structure Science, High Energy Accelerator Research Organization (KEK),*
1-1 Oho, Tsukuba 305-0801, Japan
[5]*Materials Research Center for Element Strategy (MCES), Tokyo Institute of Technology, Yokohama 226-8503, Japan*
[6]*Institute of Multidisciplinary Research for Advanced Materials, Tohoku University, 2-1-1 Katahira, Aoba-ku, Sendai 980-8577, Japan*
[7]*Synchrotron X-ray group and Synchrotron X-ray Station at SPring-8, National Institute for Materials Science (NIMS),*
Sayo, Hyogo 679-5148, Japan

(Received 18 December 2018; revised manuscript received 30 March 2019; published 13 June 2019)

We report on magnetic and electronic properties of the *B*-site-ordered double-perovskite La_2CrMnO_6 films grown by pulsed-laser deposition. The magnetic-field dependence of magnetization curves showed hysteresis at low temperatures regardless of the degree of Cr/Mn order and the saturation magnetization became smaller for the higher-Cr/Mn-ordered film. The x-ray absorption spectroscopy and x-ray magnetic circular dichroism measurements suggested antiferromagnetic coupling between Cr^{3+} and Mn^{3+} ions, resulting in ferrimagnetism of the *B*-site-ordered double-perovskite La_2CrMnO_6. A band structure was established by combining these results together with the synchrotron-radiation photoemission and optical spectra. We discuss the magnetic states among the *B*-site-ordered $La_2B'MnO_6$ (B': $3d$ transition-metal elements from V to Ni) being basically consistent with the Kanamori-Goodenough rule.

DOI: 10.1103/PhysRevB.99.235129

I. INTRODUCTION

Double-perovskite oxides ($A_2B'B''O_6$, where A is alkali-earth and/or rare-earth ions and B' and B'' are different transition-metal ions) often exhibit naturally ordered structures; $B'O_6$ and $B''O_6$ octahedra form a NaCl-type sublattice. The spontaneous ordering in thermodynamically stable phase requires large differences in the formal valence and ionic radii between B' and B'' ions [1,2]. Superexchange interaction between B' and B'' ions via adjacent oxygen ions can cause rich magnetic properties in natural superlattices as well as artificially engineered ones, providing theoretical subjects originally proposed by Kanamori and Goodenough [3–5].

Among a large variety of double-perovskite oxides, $La_2B'MnO_6$ ($B' = 3d$ transition-metal elements except for Mn) have attracted much attention because of rich magnetic functionality in the parent compound of perovskite manganites [5–8]. La_2MnNiO_6 and La_2MnCoO_6 are most popular since they form the *B*-site-ordered structures in bulk exhibiting ferromagnetic insulating nature [9–11]. In contrast, other $La_2B'MnO_6$ (B' = V, Cr, and Fe) do not form *B*-site-ordered structures in bulk [12–18]. As for La_2VMnO_6 and La_2MnFeO_6, however, the *B*-site-ordered structures have been already achieved using nonequilibrium synthesis of pulsed-laser deposition (PLD) technique [19–22]. Therefore, only La_2CrMnO_6 (LCMO) has not been synthesized in the form of the *B*-site-ordered double-perovskite structure yet.

The *B*-site-*disordered* $LaCr_xMn_{1-x}O_3$ bulks were explicitly investigated [13–16]. Because of the identical electronic configuration between Cr^{3+} and Mn^{4+}, ferromagnetic double-exchange interaction was anticipated in $LaCr_xMn_{1-x}O_3$ (Mn^{3+}/Cr^{3+}) taking ferromagnetism of $La_{1-x}Sr_xMnO_3$ (Mn^{3+}/Mn^{4+}) into account [6,16,17]. In fact, slight substitution of Mn sites with Cr ions decreased resistivity and increased Curie temperature [13–16,23]. In contrast, the large amount of substitution weakened the double-exchange interaction and the superexchange interaction governed physical properties of $LaCr_xMn_{1-x}O_3$ [14,15]. However, the random distribution of the *B*-site ions made it difficult to discuss the exchange interaction between the nearest neighbor Cr/Mn ions.

In this paper, we reported on synthesis of *B*-site-ordered double-perovskite LCMO in the form of a thin film and investigated its magnetic and electronic properties. The Cr/Mn-ordered structure was revealed from x-ray diffraction (XRD) using Cu Kα_1 and synchrotron x rays. The saturation

---

[*] Present address: Institute of Multidisciplinary Research for Advanced Materials, Tohoku University, 2-1-1 Katahira, Aoba-ku, Sendai 980-8577, Japan; kohei.yoshimatsu.c6@tohoku.ac.jp

[†] Present address: Department of Materials Molecular Science, Institute for Molecular Science, Myodaiji-cho, Okazaki, Aichi 444-8585, Japan.

[‡] Present address: Graduate School of Material Science, University of Hyogo, 3-2-1, Koto, Kamigori-cho, Ako-gun, Hyogo 678-1297, Japan.

magnetization (M_s) and magnetic transition temperature (T_C) were estimated using magnetic properties measurement systems (Quantum design, MPMS). The electrical resistivity of the films was analyzed by a thermionic emission model. The valence states of Cr and Mn ions were verified from x-ray absorption spectroscopy (XAS). The spin-spin coupling between Cr and Mn was investigated using x-ray magnetic circular dichroism (XMCD) measurements. Photoemission spectroscopy (PES) including resonant photoemission technique and O 1*s* XAS revealed the electronic structures near the Fermi level (E_F). Successful growth and elucidation of the physical properties for the *B*-site ordered LCMO completed a series of $La_2B'MnO_6$ (B': 3*d* transition-metal elements from V to Ni), which allowed us to discuss the electronic and magnetic states systematically.

II. EXPERIMENTS

The LCMO ceramic tablet was prepared by a conventional solid-state reaction method. Regent-grade La_2O_3 powder (3N) was preheated at 1000 °C for 12 h to remove moisture. Then, La_2O_3, Cr_2O_3 (3N), and MnO_2 (3N) powders with stoichiometric proportion were mixed and pressed into a pellet. It was first fired at 1000 °C for 12 h. The ceramic tablet was ground and pressed into a pellet again. Finally, it was sintered at 1200 °C for 24 h. The powder XRD measurements using Cu Kα x-ray showed only a single perovskite phase (see Fig. S1 in the Supplemental Material [24]), suggesting the known disorder bulk phase [13–17].

Prior to film growth, $SrTiO_3$ (STO) (111) substrates were treated by washing and annealing. As-received STO (111) substrates were washed with acetone and ethanol in an ultrasonic bath, then annealed in air for 3 h at 1000 °C. The annealed substrates were etched in hot water at ~50 °C to remove the segregated SrO_x. The etched substrates clearly showed a step-and-terrace structure. The LCMO films with their thickness of ~300 nm were grown on the STO (111) substrates in an ultrahigh-vacuum chamber. KrF excimer laser pulses (10 Hz, $1.7\,\mathrm{J\,cm^{-2}}$) were focused on the LCMO ceramic tablet. The growth temperature (T_g) was set constant in a range from 600 to 1000 °C. Oxygen pressure (P_{O2}) in the PLD chamber was fixed in a range from 1×10^{-6} to 0.1 Torr with the continuous flow of pure oxygen (6N purity). Note that these T_g-P_{O2} conditions are typical for PLD growth of perovskite manganites except for T_g higher than ~800 °C. After the growth, the samples were quenched to room temperature ($50\,^\circ\mathrm{C\,min^{-1}}$ in average), followed by annealing in air at 600 °C for 3 h to refill residual oxygen vacancies in the films as well as in the substrates.

The epitaxial structures were characterized using a laboratory XRD apparatus with Cu Kα_1 x-ray. Synchrotron XRD measurements were also performed at the undulator beamline of BL15XU in the SPring-8. The photon energy of the incident x-ray was set at 15 keV. The intensity of *hhh* reflections was corrected by integrating rocking curve profiles scanned along the [11–2] direction of STO substrates. Surface morphology was investigated by reflection high-energy electron diffraction (RHEED) and tapping mode atomic force microscopy (AFM). Magnetic properties were measured with a MPMS. Temperature dependence of resistivity was measured by a standard four-probe method using a physical property measurement system (PPMS, Quantum Design).

XAS and PES measurements were performed at the undulator beamline of BL2A in the Photon Factory, KEK. XAS spectra were taken in total electron yield mode and photoemission spectra were recorded using an SES-2002 electron energy analyzer. The total energy resolution was set about 200 meV. E_F was referred to that of Au electrically in contact with the samples.

XMCD measurements were performed at a twin helical undulator beamline of BL23SU in the SPring-8. The helicity switching of circular polarization was operated at 1 Hz using the twin helical undulator [25]. The XMCD spectra were taken in the total electron yield mode at $T = 10$ K and $\mu_0 H = 10$ T. The magnetic field was applied parallel to the photon direction and was perpendicular to the sample surface. The magnetic field was also reversed for the helicity switching XMCD measurements to remove extrinsic geometrical effects.

III. RESULTS AND DISCUSSION

Strong growth-condition dependence of film quality was found. We mapped out the growth phases of LCMO films identified by out-of-plane XRD patterns in a T_g-P_{O2} diagram [Fig. 1(a)]. Amorphous-phase films were grown in the low-T_g and high-P_{O2} region, while secondary phase appeared together with the perovskite one when grown in the high-T_g and low-P_{O2} region. On the other hands, single-phase perovskite films were grown in moderate T_g and P_{O2} conditions at a boundary between the T_g-P_{O2} conditions where amorphous and secondary phases were grown. Moreover, the *B*-site-ordered double-perovskite phase was obtained under a wide range of T_g-P_{O2} conditions. We chose four samples [indicated by high-order, amorphous, impurities, and low-order in Fig. 1(a)] for the following XRD analysis. Figure 1(b) shows out-of-plane XRD patterns of these films. As for the high-order film, the superlattice reflections of LCMO 111 and 333 were detected at $2\theta \sim 20°$ and 60°, respectively, which indicated the formation of the *B*-site-ordered double-perovskite phase. Meanwhile, no superlattice reflections were found for the other films. For the amorphous-phase film, no film reflections were observed from the out-of-plane XRD pattern. The secondary phase whose reflection was detected at $2\theta \sim 32°$ was found in the XRD pattern of the impurity film. We selected high-order and low-order films for the following analyses.

Synchrotron XRD measurements were also performed for evaluation of the superlattice structures. Figure 1(c) shows the symmetric reflection profiles of both the high- and low-order films. The intensity of the LCMO *hhh* ($h = 1-6$) reflections was normalized by the fundamental LCMO 444 reflection. The larger intensity of LCMO odd *hhh* reflections for the high-order film suggested the higher degree of *B*-site order. In contrast, the low-order film also showed weak but clear odd reflection peaks. Although modulation of intensity reflects the *B*-site ordered structure, the degree of *B*-site order could not be quantitatively estimated only from the intensity profile because of the closer atomic scattering factors between Cr and Mn ions [22].

It is worth mentioning that the high-order sample is obtained under a rather lower-T_g condition. Previous studies on

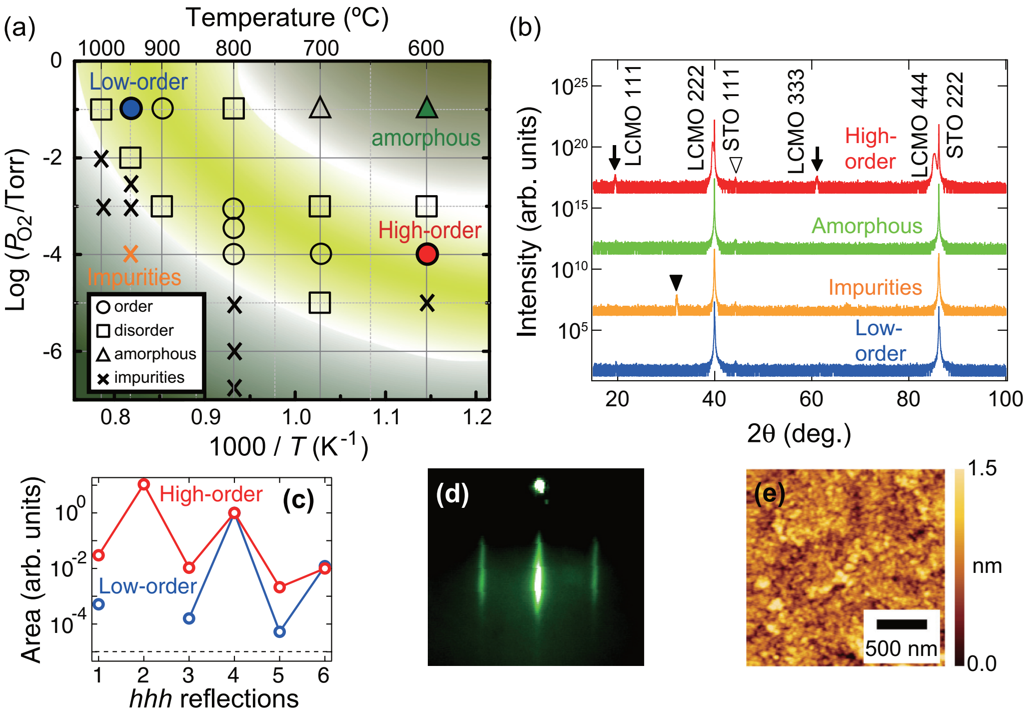

FIG. 1. (a) PLD growth conditions of LCMO films mapped in a T_g-P_{O2} diagram. The markers indicate apparent sample information determined from XRD, as *B*-site-ordered (○), disordered (□), and amorphous (Δ) phases, and mixed phases with nonperovskite secondary phases (×). The red, orange, green, and blue colors indicate representative conditions, where high-order, impurity, amorphous, and low-order films were grown, respectively. (b) Out-of-plane XRD patterns of the high-order, impurity, amorphous, and low-order films. The colors in (b) correspond to those in (a). The arrows indicate superlattice reflections. The open and filled triangles indicate the reflections coming from a sample stage and impurities, respectively. (c) Symmetric reflection profiles taken with synchrotron x rays normalized by the intensity of the 444 reflection for the high- and low-order films. The dashed line indicates the background level. (d) RHEED pattern and (e) AFM image of the high-order film.

B-site-ordered double-perovskite films indicate that the high degree of *B*-site order always requires high T_g (∼1000 °C) [19,22,26–29]. Lower-T_g and -P_{O2} conditions for LCMO were beneficial to improve surface quality of the films. The RHEED pattern of the high-order film showed strong streaks [Fig. 1(d)]. In addition, the AFM image showed flat surface with root mean square roughness of ∼0.2 nm [Fig. 1(e)].

Figure 2 shows the temperature dependence of the resistivity (ρ–T) for the high- and low-order films. Regardless of the degree of Cr/Mn order, the films showed insulating behaviors. The resistivity of the high-order film was higher by an order of magnitude than that of the low-order one in the whole range of measurement temperature. The ρ–T curves were analyzed with the thermionic emission model for the conductivity (σ). The plots of ln σ vs. $1000/T$ were well fitted to the straight lines [inset of Fig. 2] given by $\sigma = \sigma_0 \exp(-E_a/k_BT)$, where σ_0 is the pre-exponential factor, k_B is the Boltzmann constant, and E_a is an activation energy. The gradient of the fitted lines of the high-order film was slightly steeper than that of the low-order one, indicating that E_a of the high-order film (24 meV) was larger than that of the low-order film (21 meV).

Figure 3(a) shows the magnetic-field dependence of magnetization ($M-H$) taken at 5 K for the high- and low-order films. Clear hysteresis loops were observed for both films. After subtracting the diamagnetic signal from STO substrates, the M_s was estimated from the magnetizations at $\mu_0H = \pm 5$ T to be 1.1 and 2.1 μ_B/f.u. for the high- and low-order films, respectively, which were lower than that of the disorder bulk (2.3 μ_B/f.u.) [17]. Figure 3(b) shows the temperature dependence of field-cooled magnetization ($M-T$) for both films taken under $\mu_0H = 1$ T. The magnetizations were normalized at 5 K for easy comparison between the films. The inset shows the temperature dependence of the inverse magnetization ($1/M$), where T_Cs were estimated to be 100 and 140 K for the high- and low-order films, respectively, from the intercepts of the fitted lines. These T_Cs are lower than that of the disorder bulk (190 K) [17]. Moreover, these results indicate a negative correlation between magnetic properties (M_s and T_C) and the degree of Cr/Mn order, which is also found in La_2MnFeO_6 [22].

In order to investigate the valence of Cr and Mn ions, we performed XAS measurements. Figure 4(a) shows Cr 2*p* XAS spectra of the films together with the reference spectra of CrO_2(Cr^{4+}), Cr_2O_3 (Cr^{3+}), and CrF_2 (Cr^{2+}) [30]. The spectral shape of the films was quite similar to each other. The L_3 edge had a peak at around 578 eV and the L_2 edge mainly consisted of two peaks. These characteristics were consistent with the Cr^{3+} reference spectrum (Cr_2O_3), indicating that the Cr ions were trivalent in the octahedral crystal field (t_{2g}^3, e_g^0), irrespective of the degree of Cr/Mn order. Figure 4(b) shows Mn 2*p* XAS spectra of the films together with the reference spectra of MnO_2 (Mn^{4+}), $LaMnO_3$ (Mn^{3+}), and MnO (Mn^{2+}) [31]. The spectral shape of the films was also quite similar to each other. The spectra exhibited the prominent structures

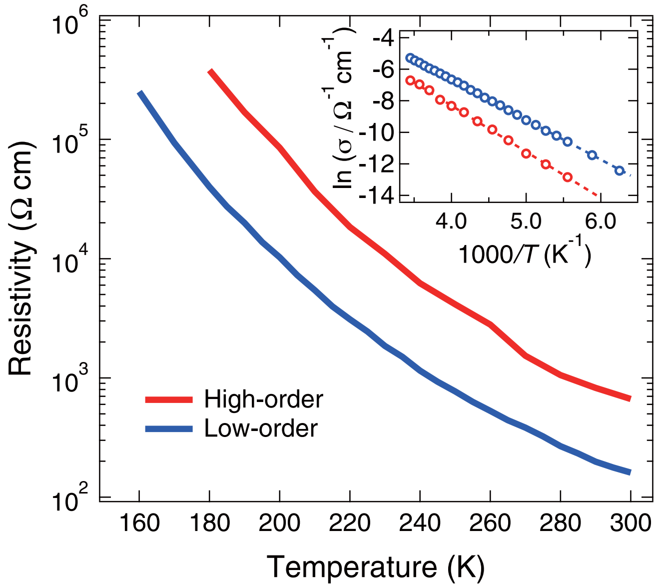

FIG. 2. Temperature dependence of the resistivity for the high- (red) and low-order (blue) LCMO films. The inset depicts ln σ plotted as a function of $1000/T$, and linear fits (dashed lines) that are based on the thermionic emission model.

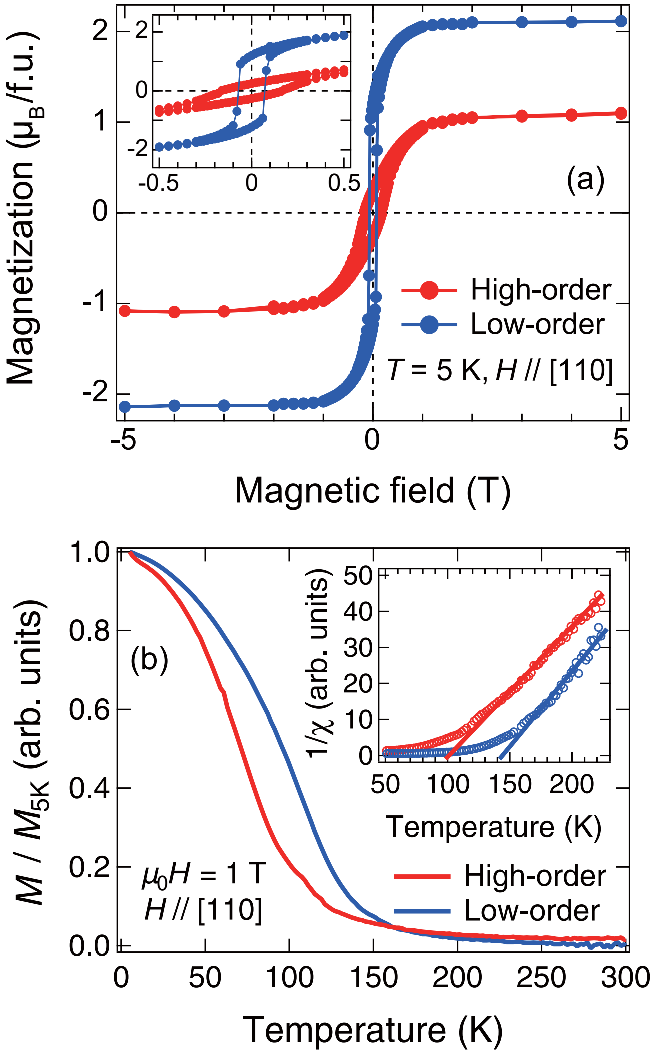

FIG. 3. (a) Magnetization hysteresis curves taken at 5 K for the high- (red) and low-order (blue) films. The magnetic field was applied parallel to the film surface. The inset shows magnification around the origin. (b) Temperature dependence of field-cooled magnetization for the same films taken during warming under $\mu_0H = 1$ T. The magnetizations are normalized by those at 5 K. The inset depicts the temperature dependence of inverse magnetization. Solid lines are linear fits to the plots.

centered at around 643 and 653 eV corresponding to the L_3 and L_2 edges, respectively, which was consistent with the Mn^{3+} reference spectrum ($LaMnO_3$), indicating that the Mn ions were also trivalent with a high-spin configuration (t_{2g}^3, e_g^1), again irrespective of the degree of Cr/Mn order.

Figure 5(a) shows Mn $2p$ XMCD spectrum of the high-order LCMO film. The strong negative XMCD signals were observed in the L_3 edge, indicating the parallel alignment between Mn $3d$ spins and the magnetic field. In contrast, the Cr $2p$ XMCD spectrum [Fig. 5(b)] showed the positive XMCD signals, indicating antiparallel alignment between Cr $3d$ spins and the magnetic field. The opposite signals between Mn $2p$ and Cr $2p$ XMCD spectra indicated the antiparallel spin configuration, suggesting ferrimagnetism in B-site-ordered double-perovskite LCMO. The XAS spectra taken using positive and negative helicity photons are shown in Fig. S4 in the Supplemental Material [24]. It is known that the element-selective magnetization can be estimated from the XMCD sum rule [32]. However, the XMCD signals were much smaller than those expected from Cr $3d$ and Mn $3d$ electronic configurations (see the Supplemental Material [24]). This is presumably due to the difference between volume and surface sensitive measurements [superconducting quantum interference device (SQUID) and XMCD, respectively]. Nevertheless, the ferrimagnetic ground states were evidently confirmed from the XCMD measurements.

We discuss the magnetic ground states of LCMO systems. From the XAS spectra (Fig. 4), Mn and Cr ions are in trivalent states. When the antisite defects occur to a perfectly ordered La_2CrMnO_6 film, the nearest neighbor $Cr^{3+}-Cr^{3+}$ and $Mn^{3+}-Mn^{3+}$ pairs are magnetically coupled by antiferromagnetic superexchange interaction. When the degree of B-site order decreases, M_s also decreases owing to the antisite defects. However, this simple description is not established in La_2CrMnO_6 because the disorder La_2CrMnO_6 exhibits the larger M_s than the ordered one [17]. In Ref. [17], Barrozo *et al.* reported M_s of 2.3 μ_B/f.u. in the disorder La_2CrMnO_6 bulk polycrystalline sample, which was larger than M_s of both high-order (1.1 μ_B/f.u.) and low-order (2.1 μ_B/f.u.) films. They suggested the parallel spin alignment of $Cr^{4+}(3d^2, S = 1)$ and low-spin Mn^{2+} $(3d^5, S = 1/2)$, and ideal saturation magnetization of 3 μ_B/f.u. in the disorder La_2CrMnO_6. The valence of both Cr and Mn ions and spin alignment were completely inconsistent with XAS and XMCD results of our high-order sample.

Within the precondition of Cr^{3+} and Mn^{3+}, the double-exchange interaction between Cr^{3+} and Mn^{3+} is a possible scenario to create magnetization in the disorder (low-order) La_2CrMnO_6. The double-exchange-like ferromagnetic

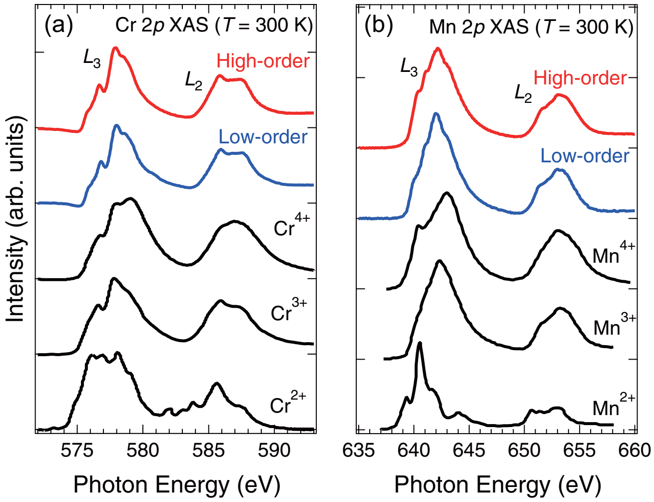

FIG. 4. (a) Cr $2p$ XAS spectra taken at 300 K for the high- (red) and low-order (blue) LCMO films. The spectra of Cr^{2+} (CrF_2), Cr^{3+} (Cr_2O_3), and Cr^{4+} (CrO_2) are also shown as references [29]. (b) Mn $2p$ XAS spectra taken at 300 K for the high- (red) and low-order (blue) LCMO films. The spectra of Mn^{2+} (MnO), Mn^{3+} ($LaMnO_3$) and Mn^{4+} (MnO_2) are also shown as references [30].

interaction was suggested for the slight substitution of Mn sites with Cr ions in $LaMnO_3$ [13–17]. If Mn-rich $LaCr_xMn_{1-x}O_3$ ($x < 0.5$) domains had been formed in the disorder La_2CrMnO_6, a sign of ferromagnetic interaction would have been observed by the SQUID measurements. The magnetization in the low-order La_2CrMnO_6 film may be explained by the Mn-rich domains. However, nevertheless, such a scenario cannot be applied to the high-order La_2CrMnO_6 film. When the double-exchange-like ferromagnetic interaction occurs, Mn $3d$ and Cr $3d$ spins should be aligned parallel to each other, which is inconsistent with the XMCD results (Fig. 5). Within the precondition of antiparallel alignment between Mn $3d$ and Cr $3d$ spins, we conclude that the antiferromagnetic superexchange interaction between Cr^{3+} and Mn^{3+} is the plausible origin of ferrimagnetism in the high-order La_2CrMnO_6 film.

The degree of B-site order can be estimated from M_s. Using M_s of the disorder La_2CrMnO_6 (2.3 μ_B/f.u.) [17] and the ideal M_s of perfectly ordered ferrimagnetic La_2CrMnO_6 (1.0 μ_B/f.u.), we simply presume the degree of the Mn/Cr order [19,21,22]. M_s of the high- and low-order La_2CrMnO_6 films is 1.1 and 2.1 μ_B/f.u. (Fig. 3), and the calculated degree of Cr/Mn order is 92 and 15%, respectively. We stress that they are approximate values assuming the uniform quality of the films. Meanwhile, as discussed in the XMCD spectra, the spin magnetic moments obtained from the sum rule are much smaller than the ideal ones, implying the existence of magnetic dead-layer at the surface of the film.

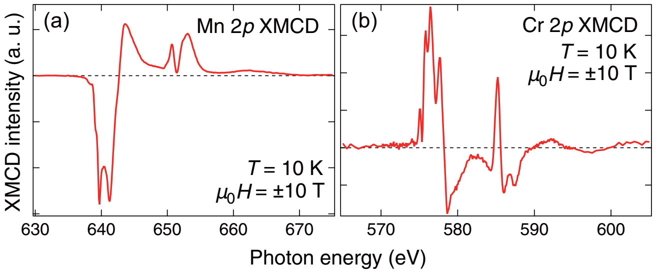

FIG. 5. (a) Mn $2p$ and (b) Cr $2p$ XMCD spectra of the high-order LCMO film taken at 10 K. The XMCD spectra were obtained from the average taken at $\mu_0 H = \pm 10$ T.

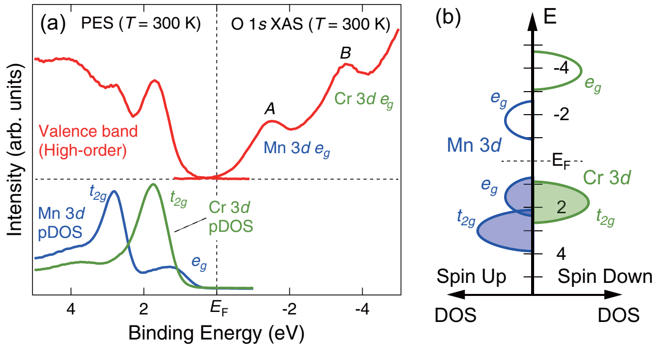

FIG. 6. Electronic structures of the high-order LCMO film. The green and blue colors in (a) and (b) indicate the Cr $3d$ and Mn $3d$ derived states, respectively. (a) Valence band and O $1s$ XAS spectra, and pDOS of Cr and Mn $3d$ obtained from resonant photoemission technique. (b) Schematic spin-resolved energy diagram of Cr and Mn $3d$ states.

Next, we discuss the electronic structures of the B-site ordered LCMO. Figure 6(a) shows the valence band and O $1s$ XAS spectrum. The energy scale for the latter is shifted so that its pre-edge with respect to the valence band maximum matched with a bandgap of 1.0 eV determined from the optical absorption measurements (see Fig. S2 in the Supplemental Material [24]). The wide-range O $1s$ XAS spectrum was also shown in Fig. S3 in the Supplemental Material [24]. In the valence band spectrum, O $2p$ derived states were located around 4–5 eV. In addition, there are sharp structures centered at 2.8 and 1.7 eV. In order to identify these features, Cr and Mn $2p$–$3d$ resonant photoemission measurements were conducted and the partial density of states (pDOS) of Cr and Mn $3d$ were obtained by subtraction of off- from on-resonant photoemission spectra. The Cr $2p$–$3d$ on- and off-resonant photoemission spectra were taken at the incident photon energy of 580.8 and 570.8 eV, respectively, and Mn $2p$–$3d$ on- and off-resonant spectra were taken at 645.9 and 635.9 eV, respectively [33,34]. In the Cr $3d$ pDOS, the peak centered at 1.7 eV was strongly enhanced, and thus could be assigned to the Cr $3d$ t_{2g} states. Similarly, the peaks centered at 2.8 and 1.3 eV were assignable to the Mn $3d$ states. Compared with photoemission spectra of hole-doped perovskite manganites [34,35], the deeper and shallower peaks could be assigned to the Mn $3d$ t_{2g} and e_g states, respectively. These resonant photoemission results indicate that the top of the valence band is dominated by the Mn $3d$ e_g states.

In the O $1s$ XAS spectrum, two peaks labeled A and B were located at ~ -2 and -4 eV, respectively. The energy differences between the edge of the Mn $3d$ e_g occupied states and peak A and between the edge of the Cr $3d$ t_{2g} occupied states and peak B were 1.0 and 3.1 eV. These values approximately correspond to the charge-transfer gap of $LaMnO_3$ (1.1 eV) and $LaCrO_3$ (3.4 eV), respectively [36]. Therefore, the features of

TABLE I. Summary of valence of B' and Mn ions and magnetic properties in $La_2B'MnO_6$ (B' = V, Cr, Mn, Fe, Co, and Ni). K–G and Exp. denote the Kanamori-Goodenough rule and experiments, respectively. FM, FiM, and AFM denote ferromagnetism, ferrimagnetism, and antiferromagnetism, respectively.

B'	Mn	Magnetic order		M_s (μ_B/f.u.)		Ref.
		K–G	Exp.	K–G	Exp.	
V^{3+} d^2	Mn^{3+} d^4	FiM	FiM	2.0	1.9	Ref. [19]
Cr^{3+} d^3	Mn^{3+} d^4	FiM	FiM	1.0	1.1	This work
Mn^{3+} d^4	Mn^{3+} d^4	AFM	AFM	0	0	Ref. [37]
Fe^{3+} d^5	Mn^{3+} d^4	FM	FiM/FM	9.0	1.3/3.0	Refs. [22,21]
Co^{2+} d^7	Mn^{4+} d^3	FM	FM	6.0	5.7	Ref. [10]
Ni^{2+} d^8	Mn^{4+} d^3	FM	FM	5.0	4.6	Ref. [11]

peaks *A* and *B* arise from Mn 3*d* e_g and Cr 3*d* e_g unoccupied states, respectively. The unoccupied Mn 3*d* e_g states may be located around peak *B* as expected from theoretical calculation although they are not experimentally observed in the O 1*s* XAS spectrum of $LaMnO_3$ single-crystal samples [37].

The O 1*s* XAS spectrum revealed that the bottom of the conduction band was also dominated by the Mn 3*d* e_g states. We summarize the spin-resolved Cr 3*d* and Mn 3*d* electronic states in Fig. 6(b). Note that part of unoccupied Mn and Cr 3*d* states smeared with other states in the O 1*s* XAS spectrum (Fig. S3) is not described in Fig. 6(b) because of ambiguity of its energy position. From the XAS measurements (Fig. 4), both Cr and Mn ions were trivalent and Mn ions had high-spin configuration. The ordering of local spin moments between Cr 3*d* and Mn 3*d* were antiparallel as verified by XMCD measurements (Fig. 5). Both the valence band maximum and the conduction band minimum were dominated by Mn 3*d* e_g states, whose energy gap was 1.0 eV, corresponding to the bandgap of $LaMnO_3$.

Successful growth of *B*-site-ordered double-perovskite LCMO enables systematic discussion on the magnetic ground states of the $La_2B'MnO_6$ system. Valences of B' and Mn ions, magnetic order, and M_s predicted from Kanamori-Goodenough (K–G) rule [3–5] and obtained from experiments [9–11,19–22,38] are listed in Table I. The magnetic orders of *B*-site-ordered $La_2B'MnO_6$ are classified into two groups. The first group consists of La_2MnCoO_6 and La_2MnNiO_6, which form the *B*-site-ordered structure in bulk, exhibits ferromagnetism [9–11]. In contrast, the second group with La_2VMnO_6, LCMO, and La_2MnFeO_6, which forms the *B*-site-disordered structure in bulk [12–18], exhibits ferrimagnetism [19,22]. The valences of transition-metal ions follow this classification of magnetism. For $La_2B'MnO_6$ with the ferromagnetic order, the valences of Mn and B' ions are +4 and +2, respectively [$Mn^{4+}(d^3)-Co^{2+}(d^7)$ and $-Ni^{2+}(d^8)$]. Meanwhile, for $La_2B'MnO_6$ with the ferrimagnetic (antiferromagnetic) order, the valences of Mn and B' ions are both +3 [$Mn^{3+}(d^4)-V^{3+}(d^2)$, $-Cr^{3+}(d^3)$, and $-Fe^{3+}(d^5)$].

In the K–G rule, a type of the 180° superexchange interaction (magnetic orders) is associated with the number of electrons filling the *d* shells for the nearest neighbor cation pairs [3–5]. In addition, M_s of B' and Mn ions can simply be roughly estimated from the spin-only magnetic moment since the orbital magnetic moment is small for 3*d* transition-metal ions except for Co ions. On the other hand, the degree of B'/Mn order has been rarely revealed. Therefore, quantitative assessments need some caution. Nevertheless, the expected M_s as well as magnetic order are in good agreement with the experimental results except for La_2MnFeO_6. It shows the ferrimagnetic (antiferromagnetic) order [22], but not the ferromagnetic order argued from the K–G rule. We note that La_2MnFeO_6 with $Mn^{3+}(d^4)-Fe^{3+}(d^5)$ is located at the boundary between two groups described already. Interestingly, such a discrepancy is also observed in La_2CrFeO_6 with $Cr^{3+}(d^3)-Fe^{3+}(d^5)$, which is also located near the boundary [26]. The sign of the superexchange interaction could be altered by the difference in the $B'-O-B''$ bond angle and $B'-B''$ bond length, giving rise to a contradiction between theory and experiments. In the G–K rule, the $B'-O-B''$ bond angle is supposed to be an ideal 180°. In contrast, the BO_6 octahedra tilt in actual perovskite oxides, which reduces the $B'-O-B''$ bond angle. The difference in the bond angle would alter the sign of the superexchange interaction. The $B'-B''$ bond length affects the total energy in each magnetic ground state. Miura *et al.* demonstrated theoretically that the magnetic ground states of La_2FeCrO_6 changed from ferromagnetism to ferrimagnetism with increasing Fe–Cr distance [39]. Indeed, there are reports on the observation of ferromagnetic order in the PLD grown La_2MnFeO_6 and La_2CrFeO_6 thin films [21,40]. Apart from such ambiguities near the boundary, however, we conclude that the magnetic ground states of $La_2B'MnO_6$ are basically explained according to the K–G rule. In this vein, comparison of M_s may be an alternative way to estimate the degree of *B*-site order, especially in such a system as LCMO, to which quantitative structural analysis is difficult only from the intensity profile of the *hhh* reflections owing to closer atomic scattering factors between Cr and Mn ions.

IV. CONCLUSION

In summary, we have synthesized *B*-site-ordered double-perovskite LCMO films by using PLD and investigated their crystal structures and physical properties. From the XRD analyses, the Cr/Mn order was clearly indicated from the superlattice reflections although the quantitative degree of Cr/Mn order was not estimated owing to closer atomic scattering factors of Cr and Mn ions. The LCMO films showed the magnetic hysteresis in the $M-H$ curves, irrespective of the degree of Cr/Mn order. The M_s and degree of Cr/Mn order showed a negative correlation and M_s of 1.1 μ_B/f.u. was obtained for the high-order film. The XAS spectra indicated trivalent states of Cr and Mn ions. The XMCD spectra suggested antiparallel spin configuration between Cr and Mn. The ferrimagnetic ground state of LCMO was suggested from magnetization, XAS, and XMCD measurements. PES including the resonant photoemission technique and XAS spectra revealed elemental-selective electronic states near E_F. The Mn 3*d* e_g states composed both the top of the valence band and bottom of the conduction band with the energy gap of ~1.0 eV. The magnetic ground state of *B*-site-ordered double-perovskite $La_2B'MnO_6$ was systematically discussed, leading to a conclusion that they basically obeyed the prediction of the K−G rule.

ACKNOWLEDGMENTS

The authors thank M. Azuma for magnetization measurements. This work was partly supported by MEXT Elements Strategy Initiative to Form Core Research Center and a Grant-in-Aid for Scientific Research (No. 19H02588, No. 18H03925, No. 16K17722, and No. 17K14334) from the Japan Society for the Promotion of Science Foundation. The synchrotron x-ray diffraction measurements were performed under the approval of the NIMS Synchrotron X-ray Station at SPring-8 (Proposal No. 2018A4700). The authors are also grateful to K. Yokoyama, S. Takeda, Y. Kagoshima, and J. Matsui, University of Hyogo for their technical contribution and Y. Katsuya for the technical support. The XMCD measurements were performed under the Shared Use Program of JAEA Facilities (Proposal No. 2017B-E16) with the approval of Nanotechnology Platform project supported by MEXT (Proposal No. A-17-AE-0035) at JAEA beamline BL23SU in SPring-8 (Proposal No. 2017B3843). The work at KEK-PF was done under the approval of the Program Advisory Committee (Proposals No. 2017G596 and No. 2018S2-004) at the Institute of Materials Structure Science, KEK.

[1] M. T. Anderson, K. B. Greenwood, G. A. Taylor, and K. R. Poeppelmeier, B-cation arrangements in double perovskites, Prog. Solid State Chem. **22**, 197 (1993).

[2] A. Ohtomo, S. Chakraverty, H. Mashiko, T. Oshima, and M. Kawasaki, Spontaneous atomic ordering and magnetism in epitaxially stabilized double perovskites, J. Mater. Res. **28**, 689 (2013).

[3] J. B. Goodenough, Theory of the role of covalence in the perovskite-type manganites [La, *M*(II)]MnO$_3$, Phys. Rev. **100**, 564 (1955).

[4] J. Kanamori, Superexchange interaction and symmetry properties of electron orbitals, J. Phys. Chem. Solids **10**, 87 (1959).

[5] J. B. Goodenough, A. Wold, R. J. Arnott, and N. Menyuk, Relationship between crystal symmetry and magnetic properties of ionic compounds containing Mn^{3+}, Phys. Rev. **124**, 373 (1961).

[6] A. Urushibara, Y. Moritomo, T. Arima, A. Asamitsu, G. Kido, and Y. Tokura, Insulator-metal transition and giant magnetoresistance in La$_{1-x}$Sr$_x$MnO$_3$, Phys. Rev. B **51**, 14103 (1995).

[7] *Colossal Magnetoresistive Oxides*, edited by Y. Tokura, Advances in Condensed Matter Science (Gordon and Breach, Amsterdam, 2000), Vol. 2.

[8] Y. Tokura and N. Nagaosa, Orbital physics in transition-metal oxides, Science **288**, 462 (2000).

[9] G. Blasse, Ferromagnetic interactions in non-metallic perovskites, J. Phys. Chem. Solids **26**, 1969 (1965).

[10] R. I. Dass and J. B. Goodenough, Multiple magnetic phases of La$_2$CoMnO$_{6-\delta}$ $(0 \leqslant \delta; \leqslant 0.05)$, Phys. Rev. B **67**, 014401 (2003).

[11] R. I. Dass, J.-Q. Yan, and J. B. Goodenough, Oxygen stoichiometry, ferromagnetism, and transport properties of La$_{2-x}$MnNiO$_{6+\delta}$, Phys. Rev. B **68**, 064415 (2003).

[12] J. Androulakis, N. Katsarakis, and J. Giapintzakis, Realization of La$_2$VMnO$_6$: Search for half-metallic antiferromagnetism? Solid State Commun. **124**, 77 (2002).

[13] U. H. Bents, Neutron diffraction study of the magnetic structures for the perovskite-type mixed oxides La(Mn, Cr)O$_3$, Phys. Rev. **106**, 225 (1957).

[14] R. Gundakaram, A. Arulraj, P. V. Vanitha, C. N. R. Rao, N. Gayathri, A. K. Raychaudhuri, and A. K. Cheetham, Effect of substitution of Cr^{3+} in place of Mn^{3+} in rare-earth manganites on the magnetism and magnetoresistance: Role of superexchange interaction and lattice distortion in *Ln*Mn$_{1-x}$Cr$_x$O$_3$, J. Solid State Chem. **127**, 354 (1996).

[15] O. Cabeza, M. Long, C. Severac, M. A. Bari, C. M. Muirhead, M. G. Francesconi, and C. Greaves, Magnetization and resistivity in chromium doped manganites, J. Phys.: Condens. Matter **11**, 2569 (1999).

[16] Y. Sun, W. Tong, X. Xu, and Y. Zhang, Possible double-exchange interaction between manganese and chromium in LaMn$_{1-x}$Cr$_x$O$_3$, Phys. Rev. B **63**, 174438 (2001).

[17] P. Barrozo and J. A. Aguiar, Ferromagnetism in Mn half-doped LaCrO$_3$ perovskite, J. Appl. Phys. **113**, 17E309 (2013).

[18] S. D. Bhame, V. L. Joseph Joly, and P. A. Joy, Effect of disorder on the magnetic properties of LaMn$_{0.5}$Fe$_{0.5}$O$_3$, Phys. Rev. B **72**, 054426 (2005).

[19] S. Chakraverty, K. Yoshimatsu, Y. Kozuka, H. Kumigashira, M. Oshima, T. Makino, A. Ohtomo, and M. Kawasaki, Magnetic and electronic properties of ordered double-perovskite La$_2$VMnO$_6$ thin films, Phys. Rev. B **84**, 132411 (2011).

[20] K. Ueda, H. Tabata, and T. Kawai, Atomic arrangement and magnetic properties of LaFeO$_3$ − LaMnO$_3$ artificial superlattices, Phys. Rev. B **60**, R12561 (1999).

[21] K. Ueda, Y. Muraoka, H. Tabata, and T. Kawai, Atomic ordering in the LaFe$_{0.5}$Mn$_{0.5}$O$_3$ solid solution film, Appl. Phys. Lett. **78**, 512 (2001).

[22] K. Yoshimatsu, K. Nogami, K. Watarai, K. Horiba, H. Kumigashira, O. Sakata, T. Oshima, and A. Ohtomo, Synthesis and magnetic properties of double-perovskite oxide La$_2$MnFeO$_6$ thin films, Phys. Rev. B **91**, 054421 (2015).

[23] L. Morales, R. Allub, B. Alascio, A. Butera, and A. Caneiro, Structural and magnetotransport properties of LaMn$_{1-x}$Cr$_x$O$_{3.00}$ $(0 \leqslant x \leqslant 0.15)$: Evidence of Mn^{3+}−O−Cr^{3+} double-exchange interaction, Phys. Rev. B **72**, 132413 (2005).

[24] See Supplemental Material at http://link.aps.org/supplemental/10.1103/PhysRevB.99.235129 for powder XRD pattern of LCMO target and optical spectrum, O K-edge XAS spectrum, and details of XMCD study on the high-order LCMO films.

[25] Y. Saitoh, Y. Fukuda, Y. Takeda, H. Yamagami, S. Takahashi, Y. Asano, T. Hara, K. Shirasawa, M. Takeuchi, T. Tanaka, and H. Kitamura, Performance upgrade in the JAEA actinide science beamline BL23SU at SPring-8 with a new twin-helical undulator, J. Synchrotron Rad. **19**, 388 (2012).

[26] S. Chakraverty, A. Ohtomo, D. Okuyama, M. Saito, M. Okude, R. Kumai, T. Arima, Y. Tokura, S. Tsukimoto, Y. Ikuhara, and M. Kawasaki, Ferrimagnetism and spontaneous ordering of transition metals in double perovskite La$_2$CrFeO$_6$ films, Phys. Rev. B **84**, 064436 (2011).

[27] S. Chakraverty, M. Saito, S. Tsukimoto, Y. Ikuhara, A. Ohtomo, and M. Kawasaki, Magnetic properties of Sr_2FeTaO_6 double perovskite epitaxially grown by pulsed-laser deposition, Appl. Phys. Lett. **99**, 223101 (2011).

[28] K. Nogami, K. Yoshimatsu, H. Mashiko, E. Sakai, H. Kumigashira, O. Sakata, T. Oshima, and A. Ohtomo, Epitaxial synthesis and electronic properties of double-perovskite Sr_2TiRuO_6 films, Appl. Phys. Express **6**, 105502 (2013).

[29] K. Watarai, K. Yoshimatsu, K. Horiba, H. Kumigashira, O. Sakata, and A. Ohtomo, Epitaxial synthesis and physical properties of double-perovskite oxide Sr_2CoRuO_6 thin films, J. Phys.: Condens. Mater **28**, 436005 (2016).

[30] C. Theil, J. van Elp, and F. Folkmann, Ligand field parameters obtained from and chemical shifts observed at the Cr $L_{2,3}$ edges, Phys. Rev. B **59**, 7931 (1999).

[31] C. Mitra, Z. Hu, P. Raychaudhuri, S. Wirth, S. I. Csiszar, H. H. Hsieh, H.-J. Lin, C. T. Chen, and L. H. Tjeng, Direct observation of electron doping in $La_{0.7}Ce_{0.3}MnO_3$ using x-ray absorption spectroscopy, Phys. Rev. B **67**, 092404 (2003).

[32] B. T. Thole, P. Carra, F. Sette, and G. van der Laan, X-Ray Circular Dichroism as a Probe of Orbital Magnetization, Phys. Rev. Lett. **68**, 1943 (1992).

[33] T. Yokobori, M. Okawa, K. Konishi, R. Takei, K. Katayama, S. Oozono, T. Shinmura, T. Okuda, H. Wadati, E. Sakai, K. Ono, H. Kumigashira, M. Oshima, T. Sugiyama, E. Ikenaga, N. Hamada, and T. Saitoh, Electronic structure of the hole-doped delafossite oxides $CuCr_{1-x}Mg_xO_2$, Phys. Rev. B **87**, 195124 (2013).

[34] K. Horiba, A. Chikamatsu, H. Kumigashira, M. Oshima, N. Nakagawa, M. Lippmaa, K. Ono, M. Kawasaki, and H. Koinuma, *In vacuo* photoemission study of atomically controlled $La_{1-x}Sr_xMnO_3$ thin films: Composition dependence of electronic structure, Phys. Rev. B **71**, 155420 (2005).

[35] T. Saitoh, A. E. Bocquet, T. Mizokawa, H. Namatame, A. Fujimori, M. Abbate, Y. Takeda, and M. Takano, Electronic structure of $La_{1-x}Sr_xMnO_3$ studied by photoemission and x-ray-absorption spectroscopy, Phys. Rev. B **51**, 13942 (1995).

[36] T. Arima, Y. Tokura, and J. B. Torrance, Variation of optical gaps in perovskite-type $3d$ transition-metal oxides, Phys. Rev. B **48**, 17006 (1993).

[37] D. -Y. Cho, S.-J. Oh, D. G. Kim, A. Tanaka, and J.-H. Park, Investigation of local symmetry effects on the electronic structure of manganites: Hexagonal $YMnO_3$ versus orthorhombic $LaMnO_3$, Phys. Rev. B **79**, 035116 (2009).

[38] J. Töpfer and J. B. Goodenough, $LaMnO_{3+\delta}$ revisited, J. Solid State Chem. **130**, 117 (1997).

[39] K. Miura and K. Terakura, Electronic and magnetic properties of La_2FeCrO_6: Superexchange interaction for a d^5-d^3 system, Phys. Rev. B **63**, 104402 (2001).

[40] K. Ueda, H. Tabata, and T. Kawai, Ferromagnetic superlattices, Science **281**, 1571a (1998).